HHS Public Access

Author manuscript

Cell Rep. Author manuscript; available in PMC 2019 February 07.

Published in final edited form as:

Cell Rep. 2019 January 22; 26(4): 955–968.e3. doi:10.1016/j.celrep.2018.12.102.

Alternative Lengthening of Telomeres through Two Distinct Break-Induced Replication Pathways

Jia-Min Zhang[1,4], **Tribhuwan Yadav**[1,4], **Jian Ouyang**[1], **Li Lan**[1,2], and **Lee Zou**[1,3,5,*]

[1]Massachusetts General Hospital Cancer Center, Harvard Medical School, Charlestown, MA 02129, USA

[2]Department of Radiation Oncology, Massachusetts General Hospital, Harvard Medical School, Charlestown, MA 02129, USA

[3]Department of Pathology, Massachusetts General Hospital, Harvard Medical School, Boston, MA 02114, USA

[4]These authors contributed equally

[5]Lead Contact

SUMMARY

Alternative lengthening of telomeres (ALT) is a telomerase-independent but recombination-dependent pathway that maintains telomeres. Here, we describe an assay to visualize ALT-mediated telomeric DNA synthesis in ALT-associated PML bodies (APBs) without DNA-damaging agents or replication inhibitors. Using this assay, we find that ALT occurs through two distinct mechanisms. One of the ALT mechanisms requires RAD52, a protein implicated in break-induced DNA replication (BIR). We demonstrate that RAD52 directly promotes telomeric D-loop formation *in vitro* and is required for maintaining telomeres in ALT-positive cells. Unexpectedly, however, RAD52 is dispensable for C-circle formation, a hallmark of ALT. In RAD52-knockout ALT cells, C-circle formation and RAD52-independent ALT DNA synthesis gradually increase as telomeres are shortened, and these activities are dependent on BLM and BIR proteins POLD3 and POLD4. These results suggest that ALT occurs through a RAD52-dependent and a RAD52-independent BIR pathway, revealing the bifurcated framework and dynamic nature of this process.

Graphical Abstract

*Correspondence: zou.lee@mgh.harvard.edu.

AUTHOR CONTRIBUTIONS

J.-M.Z., T.Y., and L.Z. designed the experiments. J.-M.Z., T.Y., and J.O. performed all the experiments. L.L. provided critical reagents. L.Z. supervised the project. J.-M.Z., T.Y., and L.Z. wrote the manuscript with inputs from all authors.

SUPPLEMENTAL INFORMATION

Supplemental Information includes seven figures and three tables and can be found with this article online at https://doi.org/10.1016/j.celrep.2018.12.102.

DECLARATION OF INTERESTS

The authors declare no competing interests.

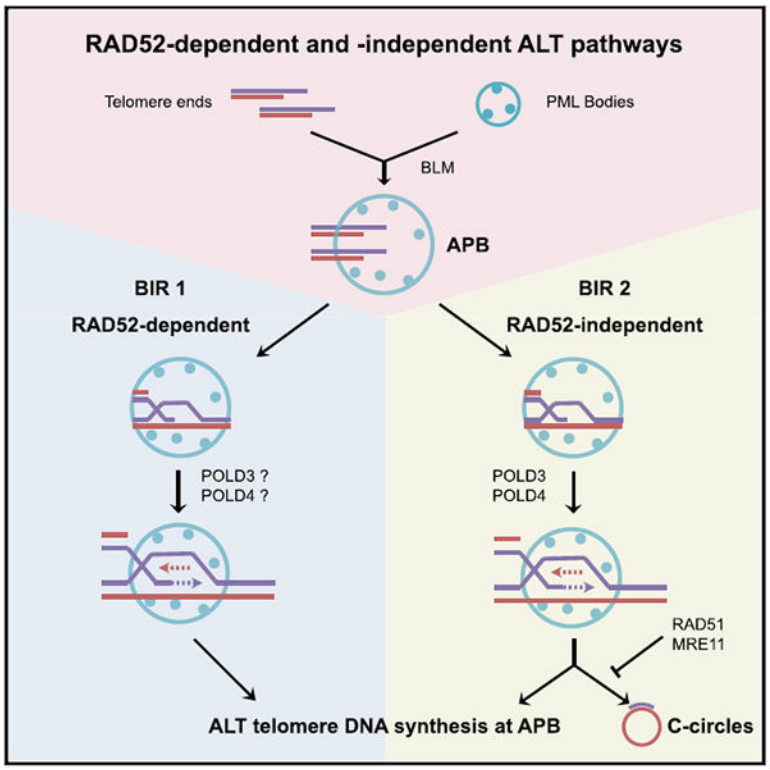

In Brief

Alternative lengthening of telomeres (ALT) is a telomerase-independent but recombination-dependent process that extends telomeres. Zhang et al. show that ALT is in fact a bifurcated pathway involving both RAD52-dependent and RAD52-independent break-induced DNA replication (BIR) in ALT-associated PML bodies (APBs), revealing an unexpected framework of the ALT pathway.

INTRODUCTION

The maintenance of telomeres is critical for the genomic stability and sustained survival of proliferating cells (Artandi and DePinho, 2010; Hanahan and Weinberg, 2011; Palm and de Lange, 2008; Verdun and Karlseder, 2007). Telomerase, an RNA-templated enzyme that extends telomeres, plays a crucial role in telomere maintenance. To bypass replicative senescence during tumorigenesis, telomerase is activated in the majority of human cancers (Shay, 2016). However, about 10%–15% of human cancers use a telomerase-independent but recombination-dependent pathway to maintain telomeres (Dilley and Greenberg, 2015; Heaphy et al., 2011; Reddel, 2014). This pathway, which is referred to as alternative lengthening of telomeres (ALT), is a potential therapeutic target in cancers lacking telomerase activity. Although a number of DNA repair and recombination proteins have been implicated in ALT, the molecular process through which ALT occurs is still poorly understood (Cesare and Reddel, 2010; Sobinoff and Pickett, 2017). Furthermore, although several common features of ALT-positive (ALT^+) cells are widely used to assess the ALT status, whether and how these ALT features are mechanistically linked to the process of ALT

remains largely unclear. A better understanding of the framework of the ALT pathway and the molecular mechanisms underlying the hallmarks of ALT will greatly facilitate the characterizations and targeting of ALT$^+$ cancers.

One of the hallmarks of ALT is ALT-associated PML bodies (APBs) (Yeager et al., 1999). In ALT$^+$ cells, APBs containing both telomeres and PML are enriched in the G2 phase of the cell cycle (Grobelny et al., 2000). High-resolution imaging studies revealed telomere clusters around PML bodies (Draskovic et al., 2009). Furthermore, a number of DNA repair and recombination proteins, including RPA, RAD51, RAD52, BLM, and others, were detected in APBs, raising the possibility that APBs provide a "recombinogenic microenvironment" to promote ALT (Acharya et al., 2014; Lillard-Wetherell et al., 2004; Nabetani et al., 2004; O'Sullivan et al., 2014; Potts and Yu, 2007; Stavropoulos et al., 2002; Wu et al., 2000; Yeager et al., 1999). Despite these tantalizing observations, it still remains unclear whether ALT DNA synthesis occurs specifically in APBs and whether APBs are essential for ALT DNA synthesis.

In addition to APBs, ALT$^+$ cells are also characteristic for harboring higher levels of extrachromosomal telomeric DNA circles, especially single-stranded C-rich circles (C-circles) (Cesare and Griffith, 2004; Henson et al., 2009; Nabetani and Ishikawa, 2009; Ogino et al., 1998; Tokutake et al., 1998; Wang et al., 2004). C-circle levels correlate with the levels of telomere DNA synthesis in ALT$^+$ cells, and high C-circle abundance is widely used as a marker for ALT activation (O'Sullivan et al., 2014; Sobinoff et al., 2017; Yu et al., 2015). Nonetheless, how C-circles are generated during ALT remains elusive.

ALT has been long speculated to be a recombination-based process (Dunham et al., 2000). In the budding yeast, the survival of telomerase null cells relies on two distinct recombination pathways (types I and II survivors) (Le et al., 1999). Although both pathways require Rad52, only one (type I survivors) depends on Rad51 (Chen et al., 2001). Both of the yeast pathways also require Pol32, a subunit of DNA polymerase d critical for break-induced DNA replication (BIR) (Lydeard et al., 2007). Recent studies in human cells further revealed that ALT is a replication stress-associated and BIR-related process. Depletion of ASF1 induces replication stress at telomeres and a spectrum of ALT-associated phenotypes (O'Sullivan et al., 2014). Induction of DNA double-strand breaks (DSBs) at telomeres elicits robust DNA synthesis through a process requiring POLD3, the counterpart of the yeast Pol32 (Dilley et al., 2016). In ALT$^+$ cells, overexpression of BLM promotes extension of telomeres in a POLD3-dependent manner (Sobinoff et al., 2017). Depletion of POLD3 or it associated partner POLD4 in ALT$^+$ cells led to a reduction in conservatively replicated telomeres, indicating their involvement in ALT (Roumelioti et al., 2016). Furthermore, the levels of mitotic DNA synthesis (MiDAS) at telomeres are elevated in ALT$^+$ cells (Min et al., 2017). Telomeric MiDAS is dependent on RAD52, which is also implicated in BIR (Bhowmick et al., 2016; Min et al., 2017;Özer et al., 2018; Sotiriou et al., 2016). Despite the similarities between ALT and BIR, some BIR factors are not required for telomere DNA synthesis in ALT$^+$ cells when analyzed with different assays (Özer et al., 2018; Sobinoff et al., 2017). Together, these findings suggest that ALT is likely triggered by replication-associated telomere breaks and occur through a BIR-like process. Although ALT is linked to BIR, it is still poorly understood as a pathway. Importantly, naturally occurring DNA

synthesis at ALT telomeres is temporally and spatially regulated during the cell cycle. Telomeric DNA synthesis was observed in G2 and mitotic ALT$^+$ cells, presenting opportunities to detect ALT activity (Dilley et al., 2016; Min et al., 2017; Nabetani et al., 2004;Özer et al., 2018; Wu et al., 2000). Assays that directly visualize the ALT DNA synthesis at unperturbed telomeres are critical for delineating the mechanisms of ALT and the cellular circuitries regulating this process.

In this study, we developed an assay to visualize telomere DNA synthesis in APBs formed in G2 human cells. The DNA synthesis detected by this assay is specific to ALT$^+$ cells and regulated by known ALT factors. Using this assay, we found that ALT DNA synthesis occurs exclusively in APBs and is dependent on PML. Furthermore, RAD52 but not RAD51 is required for efficient ALT DNA synthesis. RAD52 is not only required for maintaining telomeres in ALT$^+$ cells but also sufficient to promote telomeric D-loop formation *in vitro*, explaining its role in BIR at ALT telomeres. Surprisingly, however, RAD52 is not required for C-circle formation, suggesting the presence of a RAD52-independent ALT pathway. In RAD52-knockout cells, telomeres were progressively shortened, but C-circle formation and residual ALT DNA synthesis were gradually increased. These RAD52-independent ALT activities are dependent on BLM and POLD3/4, suggesting that the second ALT pathway is also mediated by BIR. Together, these results suggest that ALT is mediated by two BIR-related pathways, one RAD52 dependent and the other RAD52 independent. These findings establish a bifurcated framework of the ALT pathway, setting the stage for future investigations to dissect the molecular events in this process.

RESULTS

An Assay to Monitor DNA Synthesis at ALT Telomeres in APBs

To understand the process of ALT telomere DNA synthesis, we sought to visualize this process at its natural cellular location and in a cell-cycle window when it normally occurs. In particular, we sought to develop an assay to specifically monitor telomere DNA synthesis in APBs. Because in G2 cells DNA replication is largely completed throughout the genome, and APBs are readily detectable, we synchronized cells in G2 with thymidine and CDK1 inhibitor or with CDK1 inhibitor alone (Figure 1A). Using synchronized G2 cells, we performed 5-ethynyl-2′-deoxyuridine (EdU) labeling, telomere fluorescence *in situ* hybridization (FISH), and PML immunostaining. In ALT$^+$ U2OS cells, a fraction of telomeres colocalized with PML, confirming the presence of APBs (Figures 1B and S1A). In addition, a fraction of telomeres colocalized with EdU foci, showing the DNA synthesis at ALT telomeres (Figures 1B and S1A). Notably, virtually all the EdU foci in G2 U2OS cells colocalized with both telomeres and PML, suggesting that the DNA synthesis in these cells occurred primarily in APBs (Figures 1B and S1A). Similar observations were made in two other ALT$^+$ cell lines, SAOS2 and SKLU (Figure S1B). In contrast to that in ALT$^+$ cells, although PML bodies were detected in ALT− HeLa 1.3 cells synchronized in G2, they rarely colocalized with telomeres (Figures 1B and S1A). In G2 HeLa cells, EdU foci were sparse, and they very rarely colocalized with telomeres and PML (Figures 1B and S1A). Thus, by monitoring telomeres, PML and DNA synthesis simultaneously in G2 cells, we have

established an assay to visualize ALT telomere DNA synthesis in APBs. We termed this assay ATSA (ALT telomere DNA synthesis in APBs).

The ATSA assay allowed us to examine the association of APBs with ALT telomere DNA synthesis. In U2OS cells, although most of the EdU^+ telomeres were in APBs, a significant fraction of APBs did not display detectable EdU signals (Figure 1C), suggesting that telomere DNA synthesis is either not initiated or insufficient in some APBs. Interestingly, EdU^+ APBs displayed more telomere FISH signals than did EdU^-APBs (Figure S1C). Furthermore, in EdU^+ APBs, the signals of telomere FISH, PML, and EdU all positively correlated with one another (Figure S1D). These results suggest that the extents of telomere clustering in APBs are likely linked to the levels of ALT telomere DNA synthesis.

Because EdU^+ telomeres were almost exclusively detected in APBs (Figure 1C), we asked whether the lack of EdU^+ telomeres outside of APBs is due to the low abundance of telomeric DNA at non-APB telomere foci. We selected a group of telomere foci of similar sizes in or out of APBs and compared their EdU signals (Figure S1E). Even in this size-normalized population of telomere foci, EdU signals were still exclusively detected in APBs, suggesting that telomeres outside of APBs do not synthesize DNA efficiently. The strong association of EdU^+ telomeres with APBs indicates that APBs may be involved in ALT activity. To test this possibility, we used two independent small interfering RNAs (siRNAs) to knock down PML, a key structural component of APBs (Figure S1F). Depletion of PML eliminated APBs and drastically reduced EdU^+ telomeres (Figures 1D and 1E), showing that APBs are indeed functionally important for ALT telomere synthesis.

To further validate the ATSA assay, we used it to test several known regulators of ALT. The BLM helicase is implicated in APB formation and ALT DNA synthesis (O'Sullivan et al., 2014; Sobinoff et al., 2017). In U2OS cells, depletion of BLM with two independent siRNAs drastically reduced APBs and DNA synthesis at telomeres in G2 (Figures 1F, S1G, and S1H). The BIR proteins POLD3 and PODL4 are also involved in ALT (Roumelioti et al., 2016; Sobinoff et al., 2017). Knockdown of POLD3 and PODL4 in U2OS cells significantly reduced EdU^+ APBs but only modestly decreased total APB levels (Figures 1G, S1I, and S1J), supporting the idea that POLD3/4 are important for ALT telomere synthesis in APBs. Thus, the ATSA assay is not only capable of confirming the known genetic requirements of ALT but also revealing previously unknown regulatory mechanisms.

RAD52 but Not RAD51 Is Important for ALT Activity in APBs

Both RAD51 and RAD52 are among the DNA recombination proteins detected in APBs (Yeager et al., 1999), but their functions in APBs have not been tested directly. To assess the functions of RAD51 and RAD52 in APBs, we first examined their localization in G2 U2OS cells. RAD52 but not RAD51 was detected in the majority of APBs and EdU^+ telomeres (Figures 2A, S2A, and S2B). To test whether RAD51 and RAD52 are functionally required for the DNA synthesis in APBs, we analyzed RAD51 and RAD52 knockdown U2OS cells with the ATSA assay (Figures 2B and S2C). The numbers of EdU^+ APBs, but not total APBs, were significantly reduced by knockdown of RAD52 (Figures 2B–2D). In contrast, RAD51 knockdown did not affect EdU^+ APBs or total APBs (Figures 2B–2D). To confirm these results, we generated independent RAD52-knockout (KO) cell lines using CRISPR/

Cas9 (Figure S2D). These RAD52-KO cell lines did not show significant cell-cycle alterations before extensive passaging (Figure S2E). Similar to that in RAD52 knockdown cells, the numbers of EdU^+ APBs, but not total APBs, were significantly reduced in RAD52-KO cells (Figures 2E, 2F, and S2F). Consistently, RAD52 KO reduced the fractions of APBs that were EdU^+ (Figure 2G), suggesting that RAD52 contributes to ALT telomere synthesis in APBs. Together, these results suggest that RAD52 but not RAD51 is important for ALT activity in APBs.

To further verify the effects of RAD52 KO on ALT telomere synthesis, we generated RAD52-KO cell lines that inducibly express wild-type RAD52 (Figure S2G). Induction of RAD52 in RAD52-KO cells significantly increased EdU^+ APBs (Figures 2H and S2H), confirming that RAD52 is critical for ALT telomere synthesis in APBs.

RAD52 Is Required for Telomere Maintenance in ALT^+ Cells

The role of RAD52 in the DNA synthesis in APBs prompted us to investigate whether RAD52 is required for telomere maintenance in ALT^+ cells. Using a qPCR-based method (Lau et al., 2013), we measured the overall levels of telomeric DNA in wild-type (WT) U2OS cells and cells of multiple RAD52-KO clones (Figure 3A). The levels of telomeric DNA were reduced in newly generated RAD52-KO cells compared with WT cells (Figure 3A). After 3 months of passaging, RAD52-KO cells displayed a further reduction in telomeric DNA (Figure 3A), suggesting that telomeres were progressively shortened in the absence of RAD52. The levels of telomeric DNA were even lower in a RAD52-KO clone (KO #1) that had been passaged for >6 months (Figure 3A). Nonetheless, because of the lack of early passages of KO #1, we do not know whether telomeres were shortened at the same rate as in the other clones. In contrast to that in U2OS cells, KO of RAD52 in HeLa 1.3 cells did not result in a reduction in telomeric DNA relative to WT cells even after 3 months of passaging (Figure S3A). To directly test whether telomeres were shortened in ALT^+ cells lacking RAD52, we used the telomere restriction fragment (TRF) assay to analyze cells of multiple RAD52-KO clones that had been passaged for different lengths of time (Figure 3B). Compared with WT U2OS cells, RAD52-KO cells displayed clear reductions in both the amount and length of telomeric DNA (Figure 3B). The reduction of telomeric DNA in RAD52-KO cells correlated with the length of passage time, but telomeres were eventually stabilized after extensive passaging (Figure 3B). Consistent with the TRF data, telomere FISH signals were significantly reduced at individual telomeres in RAD52-KO cells compared with WT cells (Figure 3C). The RAD52-KO cell line that has been extensively passaged also showed reductions in S-phase cells, DNA synthesis, and cell proliferation (Figures S3B and S3C). The levels of senescence in RAD52-KO cell populations also appeared to correlate with the length of passage time (Figure 3D). These results suggest that RAD52 is required for the maintenance of telomeres and proliferative fitness of ALT^+ cells.

RAD52 Overcomes the Inhibition of Telomeric ssDNA Annealing by RPA

To understand the mechanisms by which RAD52 promotes ALT telomere DNA synthesis, we expressed and purified human RAD52 from *E. coli* (Figure S4A). We also purified the human RPA complex because it might modulate the functions of RAD52 on single-stranded

DNA (ssDNA) (Figure S4B). Using these purified proteins, we asked whether RAD52 has the ability to anneal single-stranded telomeric DNA, an event allowing telomere ends to engage telomeric DNA templates. Consistent with previous studies, both RAD52 and RPA bound to ssDNA of random sequences (Figures S4A and S4B) (Grimme et al., 2010; Wold, 1997). RAD52 also promoted the annealing of ssDNA regardless of the presence or absence of RPA (Figure S4C) (Grimme et al., 2010; Keskin et al., 2014; Van Dyck et al., 2001). Both RAD52 and RPA also displayed the ability to bind ssDNA consisting of telomeric repeats (ssTelo: $[TTAGGG]_{10}$) (Figures 4A and 4B). In the absence of RPA, ssTelo annealed with its complementary strand ($[CCCATT]_{10}$) at a significant rate, and RAD52 enhanced this process (Figure 4C). Notably, in presence of RPA, ssTelo lost its ability to anneal with the complementary strand (Figure 4D). However, addition of RAD52 to the reactions enabled ssTelo to anneal with the complementary strand even in the presence of RPA (Figure 4D), showing that RAD52 overcomes the inhibition of telomeric ssDNA annealing by RPA. Thus, in the presence of RPA in APBs, RAD52 may enable single-stranded telomere ends to engage complementary telomeric sequences during BIR.

RAD52 but Not RAD51 Promotes Telomeric D-Loop Formation in the Presence of RPA

A critical step during BIR is the invasion of ssDNA ends into double-stranded DNA (dsDNA) template, a process termed D-loop formation (Anand et al., 2013). RAD51 is well known to promote D-loop formation (Raynard and Sung, 2009). Using purified RAD51 protein (Figure S5A), we confirmed that RAD51 stimulated D-loop formation on non-telomeric dsDNA (Figure S5B). However, this activity of RAD51 in promoting D-loop formation was inhibited when ssDNA was coated by RPA (Figure S5C). In contrast to RAD51, RAD52 was able to stimulate D-loop formation on non-telomeric dsDNA even when ssDNA was coated by RPA (Figure 5A), allowing us to reveal a unique activity of RAD52 and recapitulate a RAD52-mediated BIR event.

To test whether RAD52 stimulates D-loop formation on telomeric dsDNA, we performed D-loop formation assays using ssTelo and a dsDNA plasmid containing 108 TTAGGG telomeric repeats (Amiard et al., 2007). Regardless of the presence or absence of RPA, RAD52 stimulated telomeric D-loop formation in a concentration-dependent manner (Figure 5B). In addition, RAD52 accelerated the formation of telomeric D-loops in the absence and presence of RPA (Figure 5C). In contrast to RAD52, RAD51 was unable to promote telomere D-loop formation in the presence of RPA (Figure S5D). Notably, RAD52 promoted telomeric D-loop formation more efficiently in the presence of RPA (Figures 5B and 5C), probably because RPA stimulates the activity of RAD52, removes G quadruplexes from ssTelo and/or stabilizes D-loops (Grimme et al., 2010; Salas et al., 2006). Together, these results show that RAD52 but not RAD51 has the ability to promote the invasion of single-stranded telomere ends into telomeric dsDNA in the presence of RPA, providing a molecular explanation of RAD52's function in telo-mere BIR.

RAD52 Is Dispensable for C-Circle Formation

Given the importance of RAD52 for ALT telomere DNA synthesis, we asked if RAD52 is required for C-circle formation, a hallmark of ALT. Using a previously established qPCR-based method (Lau et al., 2013), we first measured the levels of telomeric DNA and C-

circles in control and BLM-knockdown U2OS cells. Compared with control cells, BLM-knockdown cells had similar levels of telomeric DNA (Figure S6A). However, after the rolling-circle amplification (RCA+) of C-circles, control U2OS cells generated much more telomeric DNA than did BLM-knockdown cells, confirming that loss of BLM reduces C-circle levels (Figure S6A; O'Sullivan et al., 2014). Surprisingly, however, knockdown of RAD52 with two independent siRNAs did not reduce C-circle levels (Figures 6A and S6B). Furthermore, the levels of C-circles were not reduced in newly generated RAD52-KO cell lines compared with WT U2OS cells (Figure 6B, left, and Figure S6C). Thus, although RAD52 is important for ALT telomere DNA synthesis, it is not required for C-circle formation. This finding is consistent with the presence of residual ALT telomere DNA synthesis in RAD52-depleted cells (Figures 2B, 2C, and 2E), suggesting that C-circles may arise from a RAD52-independent ALT pathway.

RAD52 Loss Leads to Progressive Upregulation of an Alternative ALT Pathway

While analyzing C-circles in RAD52-KO cell lines, we noted that C-circle levels were significantly elevated in RAD52-KO cell lines compared with WT U2OS cells after 3 months of passaging (Figure 6B, right, and Figure S6C). Furthermore, although ALT activity in APBs was reduced in newly generated RAD52-KO cell lines, it recovered significantly after 3 months of passaging (Figures 6C and 6D). These results suggest that RAD52 loss led to progressive upregulation of an alternative ALT pathway that generates C-circles. Notably, telomeres were progressively shortened in RAD52-KO cells during the 3 months of passaging (Figure 3A), raising the possibility that the RAD52-independent ALT pathway is more active on short telomeres, and suggesting that the RAD52-independent pathway is not sufficient to fully compensate the loss of RAD52.

The RAD52-Independent ALT Pathway Is Mediated by BLM and POLD3/4

We next investigated how the RAD52-independent ALT pathway is regulated. Knockdown of BLM in RAD52-KO cells drastically reduced APBs and EdU^+ telomeres (Figures 7A, 7B, and S7A). C-circle levels in RAD52-KO cells were also significantly reduced by BLM knockdown (Figures 7C and S7B). In accordance with its RAD52-independent role in ALT, BLM was readily detected in APBs in RAD52-KO cells (Figure S7C). Thus, BLM is critical for the RAD52-independent ALT activity. BLM depletion virtually abolished ALT telomere DNA synthesis in WT U2OS cells (Figure 1F), raising the possibility that BLM is also required for the RAD52-dependent ALT pathway. Indeed, knockdown of BLM reduced APBs and the colocalization of RAD52 with telomeres in WT U2OS cells (Figure S7D), showing that BLM controls the RAD52-dependent ALT pathway as well.

To address whether the RAD52-independent ALT pathway is also mediated by BIR, we knocked down POLD3 and POLD4 in RAD52-KO cells. Knockdown of either POL3 or POLD4 in RAD52-KO cells reduced EdU^+ APBs (Figure 7D). Furthermore, depletion of POLD3 or POLD4 reduced the levels of C-circle in RAD52-KO cells (Figures 7E and S7E). Together, these results suggest that the RAD52-independent ALT pathway is also mediated by BIR factors, revealing that ALT is in fact a bifurcated BIR-related pathway operating through a RAD52-mediated and a C-circle-generating processes.

To further test whether RAD51 is involved in the RAD52-independent ALT pathway, we knocked down RAD51 in extensively passaged RAD52-KO cells. Depletion of RAD51 did not significantly affect EdU^+ APBs (Figure S7F). Unexpectedly, however, RAD51 knockdown increased C-circle levels (Figures 7F and S7G). Similarly, depletion of the MRE11 nuclease also increased C-circle levels without altering ALT telomere synthesis (Figures 7F, S7G, and S7H). These results suggest that RAD51 and MRE11 antagonize C-circle generation and that their loss uncouples C-circle formation from DNA synthesis in the RAD52-independent pathway.

DISCUSSION

Detection of ALT Activity in APBs

Detection of ALT telomere DNA synthesis is a critical step toward understanding the ALT pathway. Several assays have been established to visualize telomere DNA synthesis in ALT^+ and ALT^- cells, and each of them has unique properties. For example, the single-molecule analysis of telomeres (SMAT) can distinguish telomere DNA replication and telomere extension (Sobinoff et al., 2017). Bromodeoxyuridine (BrdU) labeling of telomeres in G2 cells and detection of MiDAS at telomeres directly visualize telomere DNA synthesis outside of S phase (Min et al., 2017; Wu et al., 2000). Furthermore, generation of DSBs at telomeres with the TRF1-FokI fusion protein induces robust telomere DNA synthesis, providing an approach to model the effects of intrinsic telomeric DSBs (Dilley et al., 2016). When applied to ALT^+ and ALT^- cells, some of these assays are able to detect more robust telomere DNA synthesis in ALT^+ cells than in ALT^- cells, indicating ALT-associated DNA synthesis. Although all these assays have contributed to the understanding of ALT telomere DNA synthesis, they have not incorporated APBs, a hallmark of ALT^+ cells, into the analysis.

We developed the ATSA assay to complement the existing assays and to detect ALT telomere DNA synthesis specifically. The ATSA assay has three important features. First, it directly visualizes telomere DNA synthesis in APBs, detecting ALT activity in its natural cellular location. Second, it detects ALT DNA synthesis in G2, a cell-cycle window in which APBs are abundant. Finally, it detects ALT DNA synthesis in the absence of DNA-damaging agents or replication inhibitors, allowing us to study intrinsic ALT activity at telomeres. Using the ATSA assay, we show that the telomere DNA synthesis in APBs is detected only in ALT^+ cells but not ALT^- cells. Furthermore, the telomere DNA synthesis in G2 ALT^+ cells occurs exclusively in APBs, suggesting that APBs are necessary for the natural ALT activity. Consistent with this idea, we show that PML is critical for ALT telomere synthesis. Additionally, *de novo* formation of APBs in ALT^+ cells induced telomere DNA synthesis and elongation (Chung et al., 2011). Prolonged knockdown of PML in ALT^+ cells resulted in telomere shortening (Osterwald et al., 2015). Although APBs are important for ALT, only the subset of APBs with high levels of telomeric DNA is associated with significant DNA synthesis, suggesting that the extents of telomere clustering in APBs are linked to ALT activity.

Although ATSA provides a useful tool to study ALT telomere synthesis, it has notable limitations. ATSA specifically analyzes ALT in G2 cells. Furthermore, ATSA cannot

distinguish DNA synthesis on a single telomere, multiple telomeres, or extrachromosomal circles. In future studies, it is important to investigate whether the regulatory mechanisms revealed by ATSA can be applied to other cell-cycle phases and to different modes of DNA synthesis at ALT telomeres.

A Bifurcated ALT Pathway

Although the ALT pathway has been extensively studied, the framework for this pathway has not yet fully emerged. Recent studies have suggested that ALT is a BIR-related pathway involving POLD3 and POLD4 (Min et al., 2017; Roumelioti et al., 2016). Furthermore, RAD52, which is also implicated in BIR, is required for the MiDAS at telomeres (Bhowmick et al., 2016; Min et al., 2017; Özer et al., 2018; Sotiriou et al., 2016). Using the ATSA assay, we found that RAD52 is indeed important for telomere DNA synthesis in APBs. We further showed that RAD52 is indispensable for the maintenance of ALT telomeres and for preventing cellular senescence. However, to our surprise, RAD52 is not required for C-circle formation, a hallmark of ALT^+ cells. This finding strongly suggests the presence of a RAD52-independent ALT pathway that generates C-circles (Figure 7G).

By combining ATSA and C-circle assays, we have gained insights into how the RAD52-dependent and RAD52-independent ALT pathways are regulated. Loss of BLM in ALT^+ cells severely compromised APB formation, telomere DNA synthesis, and C-circle generation in both the presence and absence of RAD52, suggesting that BLM is required for both ALT pathways. Given the strong effects of BLM knockdown on APBs, we speculate that BLM promotes telomere clustering upstream of both ALT pathways (Figure 7G). Our finding is consistent with the role of BLM in extending ALT telomeres and does not exclude additional functions of BLM in ALT (Sobinoff et al., 2017). In contrast to BLM, depletion of RAD51 did not significantly reduce telomere DNA synthesis in the presence or absence of RAD52, suggesting that RAD51 is not a major contributor to the two ALT pathways. However, loss of RAD51 increased C-circles, suggesting that RAD51 suppresses the C-circle generating event in the RAD52-independent pathway. Given the known roles for RAD52 and POLD3/4 in BIR, it was surprising that depletion of POLD3 and POLD4 reduced RAD52-independent telomere DNA synthesis and C-circle formation. These findings establish that both RAD52-dependent and RAD52-independent ALT pathways are BIR-related, revealing an unexpected and bifurcated framework of the ALT pathway.

Using ATSA and C-circle assays, we have also revealed interesting interplays between the two ALT pathways. C-circles were readily detected in ALT^+ cells expressing RAD52, suggesting that the RAD52-dependent and RAD52-independent pathways are active simultaneously. What controls the choice between the ALT pathways is still unknown. As telomeres became shorter in RAD52-KO cells after extensive passaging, C-circle levels were elevated, suggesting that the RAD52-independent pathway was enhanced. It is tempting to speculate that the RAD52-independent pathway is more active on short telomeres, allowing it to partially compensate the loss of RAD52 and delay senescence. Interestingly, a recent study reported that the MiDAS at telomeres was abolished by RAD52 depletion (Min et al., 2017), suggesting the absence of a RAD52-independent pathway in mitosis. Together, this finding and our data suggest that the RAD52-independent pathway may be active in G2 but

not in mitosis. These results highlight the dynamics of the ALT pathway during the cell cycle, and the unique strength of ATSA to delineate the ALT pathway.

The Role of RAD52 in Telomeric BIR

Although RAD52 has been implicated in the BIR at telomeres, the mechanism by which RAD52 functions in this process has not been elucidated. During the BIR at telomeres, the ssDNA of a telomere end needs to capture template telomeric DNA, an event requiring annealing between telomeric ssDNA. Using purified RAD52 protein, we show that RAD52 has the ability to anneal telomeric ssDNA. Importantly, RAD52 promotes telomeric ssDNA annealing in the presence of RPA, displaying an activity that RAD51 does not possess. RPA is known to localize to APBs and ALT telomeres, which may be important for establishing the recombinogenic state of ALT telomeres (Arora et al., 2014; Flynn et al., 2015) and for promoting RFC-mediated PCNA loading and subsequent Pol d function in telomere BIR (Dilley et al., 2016). The ability of RAD52 to promote telomeric ssDNA annealing in the presence of RPA may be important for telomere ends to engage DNA template and initiate BIR (Figure 7G). Consistent with this possibility, we show that RAD52 promotes telomeric D-loop formation in an RPA-stimulated manner, recapitulating the invasion of telomeric ssDNA into telomeric dsDNA during BIR. Although RAD51 is well known to promote D-loop formation, it loses this ability when telomeric ssDNA is coated by RPA. During homologous recombination (HR), BRCA2 and DSS1 enable RAD51 to overcome the inhibition by RPA (Jensen et al., 2010; Liu et al., 2010; Zhao et al., 2015). We do not exclude the possibility that RAD51 forms filaments on telomeric ssDNA *in vivo* in the presence of other proteins. However, RAD51 does not make a significant contribution to the overall ALT telomere synthesis. The different abilities of RAD52 and RAD51 to promote telomeric D-loop formation in the presence of RPA offer a possible explanation for the different contributions of RAD52 and RAD51 to ALT.

The RAD52-Independent ALT Pathway

Our experiments using RAD52-KO cells revealed the existence of a RAD52-independent ALT pathway. Surprisingly, this pathway, but not the RAD52-dependent pathway, is responsible for C-circle formation (Figure 7G). The RAD52-independent pathway involves POLD3 and POLD4, suggesting that it also operates through a BIR-related process (Figure 7G). How this BIR-related process generates C-circles is still unclear. We found that RAD51 and MRE11 antagonize C-circle formation, suggesting that RAD51 and MRE11 may suppress a certain DNA structure or a protein(s) needed for generating C-circles. Interestingly, RAD51 is required for reversal of replication forks, an event induced by replication stress (Zellweger et al., 2015), and MRE11 is involved in the nucleolytic processing of reversed forks (Hashimoto et al., 2010; Schlacher et al., 2011). Loss of RAD51 or MRE11 may prevent processing of reversed forks at telomeres, forcing stressed forks to undergo another remodeling process and generate C-circles. Consistent with this idea, loss of SMARCAL1, another protein required for fork reversal, also elevated C-circle levels (Cox et al., 2016; Poole et al., 2015). How the RAD52-independent ALT pathway is activated is still unclear. BLM depletion abolished APBs and the RAD52-independent pathway, suggesting that this pathway also operates in APBs. We speculate that the invasion of telomere ends into template DNA is mediated by a protein other than RAD52 in this

pathway. Notably, C-circle formation was enhanced when telomeres were shortened in extensively passaged RAD52-KO cells, suggesting that the RAD52-indepenent pathway is more active on short telomeres. This finding raises the possibility that the initiating event for the RAD52-independent pathway is limited by telomeres in a length-dependent manner. With the framework of the ALT pathway revealed, we are now in a position to reconstruct the pathway by further delineating the critical events in this process.

STAR★METHODS

CONTACT FOR REAGENT AND RESOURCE SHARING

Further information and requests for resources and reagents should be directed to and will be fulfilled by the Lead Contact, Dr. Lee Zou (zou.lee@mgh.harvard.edu; Massachusetts General Hospital Cancer Center, Harvard Medical School, Boston, MA, USA).

EXPERIMENTAL MODEL AND SUBJECT DETAILS

Cell culture—U2OS TRE (Lan et al., 2010), HeLa1.3, and their derivative RAD52 KO cell lines were cultured in DMEM supplemented with 10% fetal bovine serum (FBS), 2mM Glutamine and 1% penicillin/streptomycin. SAOS2 was cultured in McCoy's 5a medium supplemented with 10% FBS, 2mM Glutamine and 1% penicillin/streptomycin. SKLU1 was cultured in DMEM-F/12 medium supplemented with 10% FBS and 1% penicillin/streptomycin.

CRISPR-Cas9 KO cell lines—RAD52 was knocked out in U2OS TRE and HeLa1.3 cells using the sgRNAs previously described (Teng et al., 2018). sgRNAs (L1 CTAGGCTGGAGTCCGACCAG, and R1 ACCCACAGCAG-ACTTTCAGC) targeting the introns of *RAD52* flanking exon 4 were expressed from the PX330 vector. The gRNA-expressing plasmids were transfected into cells together with a GFP-expressing plasmid. After 5 days, top 3% GFP positive cells were sorted into 96-well plates as single cells by FACS, and grown for 2 weeks before the cells were transferred to 24-well plates. Deletion of exon 4 in the RAD52 KO clones was confirmed by PCR using primers RAD52 F and RAD52 R. Loss of RAD52 protein was verified by western blot using RAD52 antibody. The RAD52 KO clone #1 was generated in a previous study (Teng et al., 2018). The RAD52 KO clones #2 and #3 were generated in this study.

METHOD DETAILS

RNA interference—siRNA transfections were done by reverse transfection with Lipofectamine RNAiMax (Invitrogen). All siRNAs were transfected at 5 nM. For the C-circle assay, cells were collected 96 h post transfection. For synchronization using thymidine and CDK1 inhibitor (CDK1i, RO-3306), cells were treated with thymidine 48h post transfection. For synchronization using CDK1i, cells were treated with CDK1i 72h post transfection. The sequences of the siRNAs used in this study are shown in Table S1.

Cell cycle synchronization and FACS—Cells were synchronized in G2 using two methods. For synchronization using thymidine and CDK1i, cells were first treated with 2mM thymidine for 21 h, released into fresh medium for 4 h, and then treated with 15 μM

CDK1i for 12 h. For synchronization using CDK1i, cells were treated with 15 μM CDK1i for 18h. For visualization of DNA synthesis at telomere, cells were incubated with 20 μM EdU for 1h or 3h. For FACS, cells were incubated with 10 μM EdU for 30 min. EdU signals were labeled with fluorescent dye picolyl azide by click-it reaction. DNA was stained with propidium iodide.

ATSA assay—To visualize DNA synthesis at telomeres, synchronized G2 cells were incubated with 20 mM EdU for 1h or 3h. For immunofluorescence of PML, cells on coverslips were cooled on ice, rinsed once with 1× PBS, treated with pre-extraction buffer (0.1% Triton X-100, 20 mM HEPES-KOH pH 7.9, 50 mM NaCl, 3 mM MgCl2, 300 mM sucrose) for 5 min on ice, rinsed once with 1× PBS, fixed with PFA for 15 min and cold methanol (−20°C) for 10 min. Cells were then permeabilized in PBS with 0.5%Triton X-100 for 3 min, and blocked with block solution (1×PBS containing 0.05% Tween-20 and 3% BSA) for 1h at RT. Cells were incubated with primary antibody diluted in blocking solution for 2 h at RT or overnight at 4°C, washed 3 times with PBST (1×PBS containing 0.05% Tween-20), incubated with secondary antibodies conjugated to fluorophores in the same solution for 1 h at RT. Cells were then washed for 3 times with 1×PBST, stained with DAPI during the second wash. The images were captured with a Nikon 90i microscope.

For telomere FISH, PBG (0.2% [w/v] cold-water fish gelatin, 0.5% [w/v] BSA in PBS) was used as block solution. After incubation of secondary antibodies and 3 washes with PBST, cells were fixed again with PFA for 10 min at RT, dehydrated in 70%, 85%, and 100% ethanol for 2 min each, and allowed to air dry completely. Hybridizing solution (70% formamide, 2× SSC, 2 mg/ml BSA, 10% dextran sulfate) was preheated to 85°C for 5 min, and then PNA probe TelC-FITC (F1009, PNA Bio) was added to the hybridizing solution. Cells on coverslips were incubated with 20 μL preheated Hybridizing solution containing 100 nM PNA probe and denatured for 10 min at 85°C on a heat block. After 2 h incubation at RT in the dark, cells were washed three times with Wash solution (70% formamide, 2× SSC) for 5 min each and in 2× SSC, 0.1% tween-20 three times for 5 min each. During the second wash, cells were stained with DAPI. The images were captured with a Nikon 90i microscope.

C-circle assay—C-circle assay was performed as previously described (Lau et al., 2013). Genomic DNA was extracted with PureLink Genomic DNA Mini Kit (K182002). Diluted DNA (16 ng) was combined with 0.2 mg/ml BSA, 0.1% Tween, 4mM dithiothreitol (DTT), 1 mM each dNTP without dCTP, 1× φ29 Buffer (NEB) and 7.5 U φ29 DNA polymerase (NEB). Samples were incubated for 8 h at 30°C followed by 20 min at 65°C. For RCA(+) samples, the assay was done with 429 DNA polymerase. For RCA(−) samples, the assay was done without φ29 DNA polymerase. The levels of telomeric DNA in RCA(−) and RCA(+) samples were quantified by qPCR. C-circles are calculated by ΔCt (RCA+)/ΔCt (RCA−). For each control or knockdown condition, triplicated samples were used for the quantification of C-circles. The primers used in this study are shown in Table S2.

TRF assay—Genomic DNA was isolated from cells using PureLink Genomic DNA Mini Kit (K182002). Genomic DNA was digested using *Alu*I/MboI (NEB). Digested DNA (10 mg) was separated by 1% agarose gel electrophoresis using CHEF-DRII system in 0.5%

TBE buffer at 14°C for 20 h. Gel was dried for 4 h at 50°C then denatured in buffer (0.5 N NaOH 1.5 M NaCl) for 1 h and neutralized in buffer (3 M NaCl, 0.5 M Tris-HCl pH 7.0) for 30 min. Gel was pre-incubated in church buffer (40 mM sodium phosphate pH 7.2, 1 mM NaOH-EDTA pH 8.0, 1% SDS, 1% BSA) for 30 min and then hybridized by 5' radiolabeled probe $(CCCTAA)_3$ in church buffer for 20 h at 28°C. Gel was washed four times in 4× SSC buffer (0.6 M NaCl, 0.06 M sodium citrate pH 7.0) and imaged using X-ray film.

Protein Purification—For purification of human RAD52, Rosetta cells harboring pET28b-RAD52 that encodes hRAD52 with C-terminal 6× his tag were grown until OD600 reached 0.6, and induced with 0.3 mM IPTG for 3 h at 30°C. Cell pellet (10 g) was lysed in Lysis buffer [25 mM Tris-HCL (pH7.5), 500 mM KCI, 1 mM EDTA, 10% glycerol, 1 mM DTT, 0.01% Igepal, 1 mM PMSF and mixture of protease inhibitors] and sonicated. Cell lysate was centrifuged for 1 h at 16 K RPM. Cleared supernatant was diluted 5 times and loaded onto Affi-blue beads in T buffer [25 mM Tris-HCL (pH7.5), 1 mM EDTA, 10% glycerol, 1 mM DTT, 0.01% Igepal] with 100 mM KCl. By using FPLC, RAD52 protein was eluted by gradient of 0 M–2.5 M NaSCN in T buffer. Fractions containing RAD52 protein were pooled and dialyzed against T buffet with 300 mM KCI and then incubated with Ni-NTA agarose beads for 2 h. RAD52 protein was eluted by gradient of 10–300 mM imidazole in T buffer. Fractions containing RAD52 protein were pooled and dialyzed against T buffer with 300 mM KCI, concentrated and stored in −80°C for biochemical assays. Human RPA was purified as previously described (Nguyen et al., 2017). Human RAD51 was purified as previously described (Sigurdsson et al., 2001).

Electrophoresis mobility shift assay (EMSA)—Single-stranded DNA oligomers were labeled at 5' end and incubated with proteins in Buffer B [25 mM Tris-HCl (pH 7.5), 1 mM $MgCl_2$, 1 mM DTT, 50 mg/ml BSA] with 50 mM KCI for 15 min at 37°C. Reaction products were loaded onto a 6% PAGE-TBE gel and resolved at 4°C. Gels were exposed to X-ray film and analyzed.

Single-stranded DNA annealing assay—Single-stranded DNA oligomer (oligo 1) was labeled at 5' end and incubated with RAD52 and/or RPA in Buffer B [25 mM Tris-HCI (pH 7.5), 1 mM $MgCl_2$, 1 mM DTT, 50 mg/ml BSA] with 50 mM KCl. Telo C strand was 5' end labeled for telomere annealing assays. Complementary oligomer (oligo 2) was added to reactions and incubated for various length of time. After incubation, 1 mg/ml proteinase K, 0.5% SDS and 0.5 mM EDTA was added and reactions continued for 5 min at 30°C. Reaction products were resolved in 10% nondenaturing polyacrylamide gels in TAE buffer (30 mM Tris-acetate, pH 7.4, 0.5 mM EDTA) at 4°C. Gels were analyzed using X-ray film or an Odyssey scanner (LI-COR Biosciences).

D loop assay—Thirty ng of 5' end fluorescent labeled single-stranded DNA oligomer (90 nt) was incubated with the indicated proteins in buffer C (35 mM Tris-HCl, 1 mm DTT, 2 mM $MgCl_2$, 50 mg/ml BSA, 50 mM KCI) with 2 mM ATP or AMP-PNP, and/or 2 mM $CaCl_2$), and then the pBSK+ plasmid (25 nM) was added to the reactions and incubated at 30°C or 37° for the indicated length of time. For telomeric D-loop assay, 20 nM ssTelo (60 nt) and 10 nM pTELO plasmid were used. After incubation, 1 mg/ml proteinase K, 0.5%

SDS and 0.5 mM EDTA was added and reactions continued for 5 min. Reaction products were resolved in 1% agarose gel with TAE buffer. Gels were analyzed using an Odyssey scanner (LI-COR Biosciences). The oligos used in this study are shown in Table S3.

QUANTIFICATION AND STATISTICAL ANALYSIS

The colocalization of PML, EdU and telomere FISH signals was quantified manually using NIS element viewer (https://www.nikoninstruments.com/Products/Software/NIS-Elements-Advanced-Research/NIS-Elements-Viewer). For the quantification of numbers of EdU^+ APBs or EdU^+ telomeres, approximately 100 cells were analyzed. When the intensity of PML, EdU or telomere FISH foci was analyzed, the colocalization and intensity of these foci were quantified together using the FociLab 2.0 software developed by Dr. Li-Lin Du's lab. The b-Gal positive cells are quantified manually using Photoshop. For EMSA, single-stranded annealing, and D-loop assays, gels were analyzed using X-ray film or an Odyssey scanner (LI-COR Biosciences). Unpaired Student's t test is used for statistical analysis as shown in figure legends.

Supplementary Material

Refer to Web version on PubMed Central for supplementary material.

ACKNOWLEDGMENTS

We thank Dr. E. Gilson for the pTELO plasmid, Dr. P. Sung for the RAD52 expression plasmid, Dr. L.-L. Du and Ms. F. Suo for the FociLab 2.0 software, and members of the Zou and Dyson laboratories for discussions. L.Z. is the James & Patricia Poitras Endowed Chair in Cancer Research and was supported by the Jim & Ann Orr Massachusetts General Hospital Research Scholar Award. This work is supported by grants from the NIH (GM076388 and CA197779) to L.Z.

REFERENCES

Acharya S, Kaul Z, Gocha AS, Martinez AR, Harris J, Parvin JD, and Groden J (2014). Association of BLM and BRCA1 during telomere maintenance in ALT cells. PLoS ONE 9, e103819. [PubMed: 25084169]

Amiard S, Doudeau M, Pinte S, Poulet A, Lenain C, Faivre-Moskalenko C, Angelov D, Hug N, Vindigni A, Bouvet P, et al. (2007). A topological mechanism for TRF2-enhanced strand invasion. Nat. Struct. Mol. Biol 14, 147–154. [PubMed: 17220898]

Anand RP, Lovett ST, and Haber JE (2013). Break-induced DNA replication. Cold Spring Harb. Perspect. Biol 5, a010397. [PubMed: 23881940]

Arora R, Lee Y, Wischnewski H, Brun CM, Schwarz T, and Azzalin CM (2014). RNaseH1 regulates TERRA-telomeric DNA hybrids and telomere maintenance in ALT tumour cells. Nat. Commun 5, 5220. [PubMed: 25330849]

Artandi SE, and DePinho RA (2010). Telomeres and telomerase in cancer. Carcinogenesis 31, 9–18. [PubMed: 19887512]

Bhowmick R, Minocherhomji S, and Hickson ID (2016). RAD52 facilitates mitotic DNA synthesis following replication stress. Mol. Cell 64, 1117–1126. [PubMed: 27984745]

Cesare AJ, and Griffith JD (2004). Telomeric DNA in ALT cells is characterized by free telomeric circles and heterogeneous t-loops. Mol. Cell. Biol 24, 9948–9957. [PubMed: 15509797]

Cesare AJ, and Reddel RR (2010). Alternative lengthening of telomeres: models, mechanisms and implications. Nat. Rev. Genet 11, 319–330. [PubMed: 20351727]

Chen Q, Ijpma A, and Greider CW (2001). Two survivor pathways that allow growth in the absence of telomerase are generated by distinct telomere recombination events. Mol. Cell. Biol 21, 1819–1827. [PubMed: 11238918]

Chung I, Leonhardt H, and Rippe K (2011). De novo assembly of a PML nuclear subcompartment occurs through multiple pathways and induces telo-mere elongation. J. Cell Sci 124, 3603–3618. [PubMed: 22045732]

Cox KE, Maréchal A, and Flynn RL (2016). SMARCAL1 resolves replication stress at ALT telomeres. Cell Rep 14, 1032–1040. [PubMed: 26832416]

Dilley RL, and Greenberg RA (2015). ALTernative telomere maintenance and cancer. Trends Cancer 1, 145–156. [PubMed: 26645051]

Dilley RL, Verma P, Cho NW, Winters HD, Wondisford AR, and Greenberg RA (2016). Break-induced telomere synthesis underlies alternative telomere maintenance. Nature 539, 54–58. [PubMed: 27760120]

Draskovic I, Arnoult N, Steiner V, Bacchetti S, Lomonte P, and Londoño-Vallejo A (2009). Probing PML body function in ALT cells reveals spatiotemporal requirements for telomere recombination. Proc. Natl. Acad. Sci. USA 106, 15726–15731. [PubMed: 19717459]

Dunham MA, Neumann AA, Fasching CL, and Reddel RR (2000). Telomere maintenance by recombination in human cells. Nat. Genet 26, 447–450. [PubMed: 11101843]

Flynn RL, Cox KE, Jeitany M, Wakimoto H, Bryll AR, Ganem NJ, Bersani F, Pineda JR, Suvà ML, Benes CH, et al. (2015). Alternative lengthening of telomeres renders cancer cells hypersensitive to ATR inhibitors. Science 347, 273–277. [PubMed: 25593184]

Grimme JM, Honda M, Wright R, Okuno Y, Rothenberg E, Mazin AV, Ha T, and Spies M (2010). Human Rad52 binds and wraps single-stranded DNA and mediates annealing via two hRad52-ssDNA complexes. Nucleic Acids Res 38, 2917–2930. [PubMed: 20081207]

Grobelny JV, Godwin AK, and Broccoli D (2000). ALT-associated PML bodies are present in viable cells and are enriched in cells in the G(2)/M phase of the cell cycle. J. Cell Sci 113, 4577–4585. [PubMed: 11082050]

Hanahan D, and Weinberg RA (2011). Hallmarks of cancer: the next generation. Cell 144, 646–674. [PubMed: 21376230]

Hashimoto Y, Ray Chaudhuri A, Lopes M, and Costanzo V (2010). Rad51 protects nascent DNA from Mre11-dependent degradation and promotes continuous DNA synthesis. Nat. Struct. Mol. Biol 17, 1305–1311. [PubMed: 20935632]

Heaphy CM, Subhawong AP, Hong SM, Goggins MG, Montgomery EA, Gabrielson E, Netto GJ, Epstein JI, Lotan TL, Westra WH, et al. (2011). Prevalence of the alternative lengthening of telomeres telomere maintenance mechanism in human cancer subtypes. Am. J. Pathol 179, 1608–1615. [PubMed: 21888887]

Henson JD, Cao Y, Huschtscha LI, Chang AC, Au AY, Pickett HA, and Reddel RR (2009). DNA C-circles are specific and quantifiable markers of alternative-lengthening-of-telomeres activity. Nat. Biotechnol 27, 1181–1185. [PubMed: 19935656]

Jensen RB, Carreira A, and Kowalczykowski SC (2010). Purified human BRCA2 stimulates RAD51-mediated recombination. Nature 467, 678–683. [PubMed: 20729832]

Keskin H, Shen Y, Huang F, Patel M, Yang T, Ashley K, Mazin AV, and Storici F (2014). Transcript-RNA-templated DNA recombination and repair. Nature 515, 436–439. [PubMed: 25186730]

Lan L, Ui A, Nakajima S, Hatakeyama K, Hoshi M, Watanabe R, Janicki SM, Ogiwara H, Kohno T, Kanno S, and Yasui A (2010). The ACF1 complex is required for DNA double-strand break repair in human cells. Mol. Cell 40, 976–987. [PubMed: 21172662]

Lau LM, Dagg RA, Henson JD, Au AY, Royds JA, and Reddel RR (2013). Detection of alternative lengthening of telomeres by telomere quantitative PCR. Nucleic Acids Res 41, e34. [PubMed: 22923525]

Le S, Moore JK, Haber JE, and Greider CW (1999). RAD50 and RAD51 define two pathways that collaborate to maintain telomeres in the absence of telomerase. Genetics 152, 143–152. [PubMed: 10224249]

Lillard-Wetherell K, Machwe A, Langland GT, Combs KA, Behbehani GK, Schonberg SA, German J, Turchi JJ, Orren DK, and Groden J (2004). Association and regulation of the BLM helicase by the telomere proteins TRF1 and TRF2. Hum. Mol. Genet 13, 1919–1932. [PubMed: 15229185]

Liu J, Doty T, Gibson B, and Heyer WD (2010). Human BRCA2 protein promotes RAD51 filament formation on RPA-covered single-stranded DNA. Nat. Struct. Mol. Biol 17, 1260–1262. [PubMed: 20729859]

Lydeard JR, Jain S, Yamaguchi M, and Haber JE (2007). Break-induced replication and telomerase-independent telomere maintenance require Pol32. Nature 448, 820–823. [PubMed: 17671506]

Min J, Wright WE, and Shay JW (2017). Alternative lengthening of telomeres mediated by mitotic DNA synthesis engages break-induced replication processes. Mol. Cell. Biol 37, e00226–17. [PubMed: 28760773]

Nabetani A, and Ishikawa F (2009). Unusual telomeric DNAs in human telomerase-negative immortalized cells. Mol. Cell. Biol 29, 703–713. [PubMed: 19015236]

Nabetani A, Yokoyama O, and Ishikawa F (2004). Localization of hRad9, hHus1, hRad1, and hRad17 and caffeine-sensitive DNA replication at the alternative lengthening of telomeres-associated promyelocytic leukemia body. J. Biol. Chem 279, 25849–25857. [PubMed: 15075340]

Nguyen HD, Yadav T, Giri S, Saez B, Graubert TA, and Zou L (2017). Functions of replication protein A as a sensor of R loops and a regulator of RNaseH1. Mol. Cell 65, 832–847.e4. [PubMed: 28257700]

O'Sullivan RJ, Arnoult N, Lackner DH, Oganesian L, Haggblom C, Corpet A, Almouzni G, and Karlseder J (2014). Rapid induction of alternative lengthening of telomeres by depletion of the histone chaperone ASF1. Nat. Struct. Mol. Biol 21, 167–174. [PubMed: 24413054]

Ogino H, Nakabayashi K, Suzuki M, Takahashi E, Fujii M, Suzuki T, and Ayusawa D (1998). Release of telomeric DNA from chromosomes in immortal human cells lacking telomerase activity. Biochem. Biophys. Res. Commun 248, 223–227. [PubMed: 9675117]

Osterwald S, Deeg KI, Chung I, Parisotto D, Wörz S, Rohr K, Erfle H, and Rippe K (2015). PML induces compaction, TRF2 depletion and DNA damage signaling at telomeres and promotes their alternative lengthening. J. Cell Sci 128, 1887–1900. [PubMed: 25908860]

Özer Ö, Bhowmick R, Liu Y, and Hickson ID (2018). Human cancer cells utilize mitotic DNA synthesis to resist replication stress at telomeres regardless of their telomere maintenance mechanism. Oncotarget 9, 15836–15846. [PubMed: 29662610]

Palm W, and de Lange T (2008). How shelterin protects mammalian telomeres. Annu. Rev. Genet 42, 301–334. [PubMed: 18680434]

Poole LA, Zhao R, Glick GG, Lovejoy CA, Eischen CM, and Cortez D (2015). SMARCAL1 maintains telomere integrity during DNA replication. Proc. Natl. Acad. Sci. U S A 112, 14864–14869. [PubMed: 26578802]

Potts PR, and Yu H (2007). The SMC5/6 complex maintains telomere length in ALT cancer cells through SUMOylation of telomere-binding proteins. Nat. Struct. Mol. Biol 14, 581–590. [PubMed: 17589526]

Raynard S, and Sung P (2009). Assay for human Rad51-mediated DNA displacement loop formation. Cold Spring Harbor Protoc 2009,

Reddel RR (2014). Telomere maintenance mechanisms in cancer: clinical implications. Curr. Pharm. Des 20, 6361–6374. [PubMed: 24975603]

Roumelioti FM, Sotiriou SK, Katsini V, Chiourea M, Halazonetis TD, and Gagos S (2016). Alternative lengthening of human telomeres is a conservative DNA replication process with features of break-induced replication. EMBO Rep 17, 1731–1737. [PubMed: 27760777]

Salas TR, Petruseva I, Lavrik O, Bourdoncle A, Mergny JL, Favre A, and Saintomé C (2006). Human replication protein A unfolds telomeric G-quadruplexes. Nucleic Acids Res 34, 4857–4865. [PubMed: 16973897]

Schlacher K, Christ N, Siaud N, Egashira A, Wu H, and Jasin M (2011). Double-strand break repair-independent role for BRCA2 in blocking stalled replication fork degradation by MRE11. Cell 145, 529–542. [PubMed: 21565612]

Shay JW (2016). Role of telomeres and telomerase in aging and cancer. Cancer Discov 6, 584–593. [PubMed: 27029895]

Sigurdsson S, Trujillo K, Song B, Stratton S, and Sung P (2001). Basis for avid homologous DNA strand exchange by human Rad51 and RPA. J. Biol. Chem 276, 8798–8806. [PubMed: 11124265]

Sobinoff AP, and Pickett HA (2017). Alternative lengthening of telomeres: DNA repair pathways converge. Trends Genet 33, 921–932. [PubMed: 28969871]

Sobinoff AP, Allen JA, Neumann AA, Yang SF, Walsh ME, Henson JD, Reddel RR, and Pickett HA (2017). BLM and SLX4 play opposing roles in recombination-dependent replication at human telomeres. EMBO J 36, 2907–2919. [PubMed: 28877996]

Sotiriou SK, Kamileri I, Lugli N, Evangelou K, Da-Ré C, Huber F, Padayachy L, Tardy S, Nicati NL, Barriot S, et al. (2016). Mammalian RAD52 functions in break-induced replication repair of collapsed DNA replication forks. Mol. Cell 64, 1127–1134. [PubMed: 27984746]

Stavropoulos DJ, Bradshaw PS, Li X, Pasic I, Truong K, Ikura M, Ungrin M, and Meyn MS (2002). The Bloom syndrome helicase BLM interacts with TRF2 in ALT cells and promotes telomeric DNA synthesis. Hum. Mol. Genet 11, 3135–3144. [PubMed: 12444098]

Teng Y, Yadav T, Duan M, Tan J, Xiang Y, Gao B, Xu J, Liang Z, Liu Y, Nakajima S, et al. (2018). ROS-induced R loops trigger a transcription-coupled but BRCA1/2-independent homologous recombination pathway through CSB. Nat. Commun 9, 4115. [PubMed: 30297739]

Tokutake Y, Matsumoto T, Watanabe T, Maeda S, Tahara H, Sakamoto S, Niida H, Sugimoto M, Ide T, and Furuichi Y (1998). Extra-chromosomal telomere repeat DNA in telomerase-negative immortalized cell lines. Biochem. Biophys. Res. Commun 247, 765–772. [PubMed: 9647768]

Van Dyck E, Stasiak AZ, Stasiak A, and West SC (2001). Visualization of recombination intermediates produced by RAD52-mediated single-strand annealing. EMBO Rep 2, 905–909. [PubMed: 11571269]

Verdun RE, and Karlseder J (2007). Replication and protection of telomeres. Nature 447, 924–931. [PubMed: 17581575]

Wang RC, Smogorzewska A, and de Lange T (2004). Homologous recombination generates T-loop-sized deletions at human telomeres. Cell 119, 355–368. [PubMed: 15507207]

Wold MS (1997). Replication protein A: a heterotrimeric, single-stranded DNA-binding protein required for eukaryotic DNA metabolism. Annu. Rev. Biochem 66, 61–92. [PubMed: 9242902]

Wu G, Lee WH, and Chen PL (2000). NBS1 and TRF1 colocalize at promyelocytic leukemia bodies during late S/G2 phases in immortalized telomerase-negative cells. Implication of NBS1 in alternative lengthening of telomeres. J. Biol. Chem 275, 30618–30622. [PubMed: 10913111]

Yeager TR, Neumann AA, Englezou A, Huschtscha LI, Noble JR, and Reddel RR (1999). Telomerase-negative immortalized human cells contain a novel type of promyelocytic leukemia (PML) body. Cancer Res 59, 4175–4179. [PubMed: 10485449]

Yu EY, Pérez-Martín J, Holloman WK, and Lue NF (2015). Mre11 and Blm-dependent formation of ALT-like telomeres in Ku-deficient Ustilago maydis. PLoS Genet 11, e1005570. [PubMed: 26492073]

Zellweger R, Dalcher D, Mutreja K, Berti M, Schmid JA, Herrador R, Vindigni A, and Lopes M (2015). Rad51-mediated replication fork reversal is a global response to genotoxic treatments in human cells. J. Cell Biol 208, 563–579. [PubMed: 25733714]

Zhao W, Vaithiyalingam S, San Filippo J, Maranon DG, Jimenez-Sainz J, Fontenay GV, Kwon Y, Leung SG, Lu L, Jensen RB, et al. (2015). Promotion of BRCA2-Dependent Homologous Recombination by DSS1 via RPA Targeting and DNA Mimicry. Mol. Cell 59, 176–187. [PubMed: 26145171]

Highlights

- An assay to visualize ALT telomere DNA synthesis in APBs
- APBs are functionally important for ALT DNA synthesis
- RAD52 promotes telomere D-loops in vitro and ALT DNA synthesis in APBs
- A RAD52-independent BIR pathway is responsible for C-circle formation

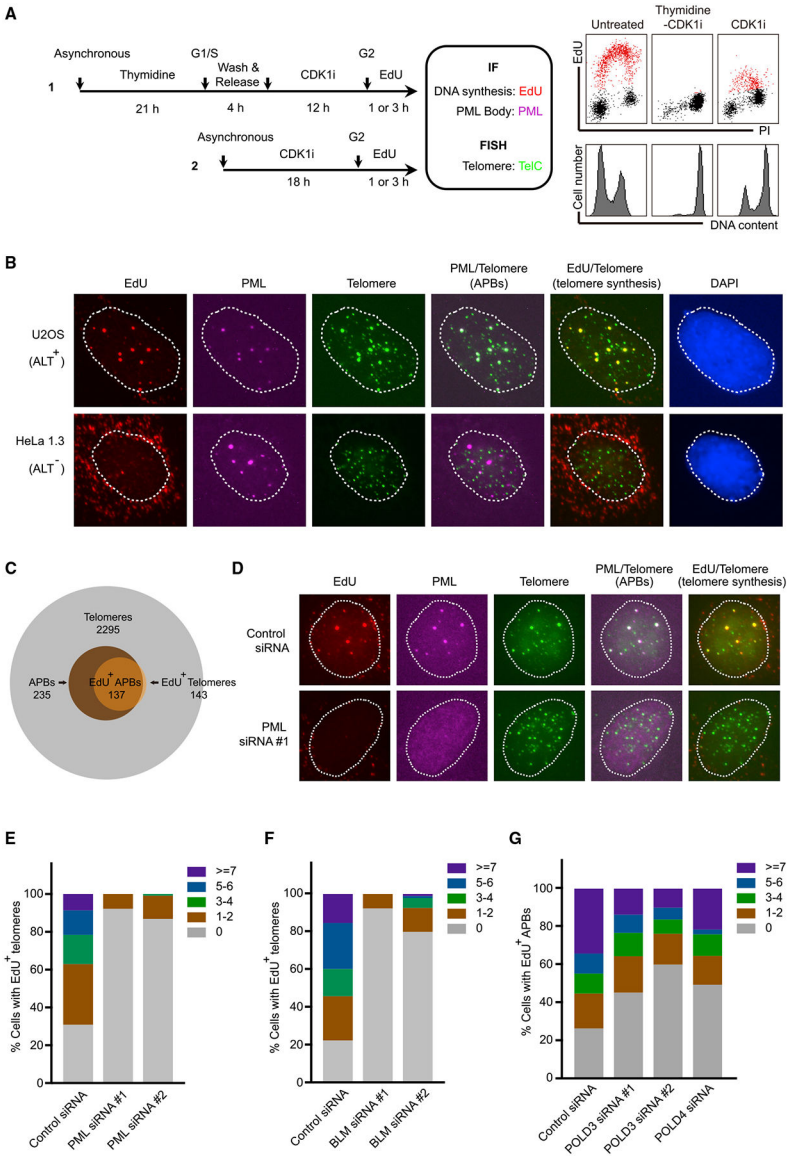

Figure 1. An Assay to Monitor DNA Synthesis at ALT Telomeres in APBs

(A) Experimental scheme for visualizing EdU incorporation in APBs in cells enriched in G2 with thymidine and CDK1i or with CDK1i. G2 cells were labeled with EdU for 1 or 3 h. EdU and PML were detected by immunofluorescence (IF), and telomeres were detected by FISH using the TelC PNA probe (left). EdU incorporation and cell-cycle profiles of the cell populations tested (right).

(B) Representative images showing the localization of EdU, PML, and telomeres at G2 U2OS (ALT^+) and HeLa1.3 (ALT^-) cells. The cells were synchronized in G2 using thymidine and CDK1i.

(C) Quantification of telomeres for their presence in APBs and EdU incorporation. The numbers of total, APB^+, and EdU^+ telomeres were determined in U2OS cells (2,295 telomeres in 42 cells were analyzed).

(D) Representative images showing the localization of EdU, PML, and telomeres in PML knockdown and control U2OS cells.
(E and F) U2OS cells were treated with control, PML (E), or BLM (F) siRNAs and synchronized in G2 using CDK1i. Approximately 100 cells were divided into five groups (0, 1 or 2, 3 or 4, 5 or 6, and ≥7) on the basis of the numbers of EdU^+ telomeres.
(G) Cells were treated with control, POLD3, or POLD4 siRNA and synchronized using thymidine and CDK1i, and 100 cells were divided into five groups on the basis of the numbers of EdU^+ APBs.

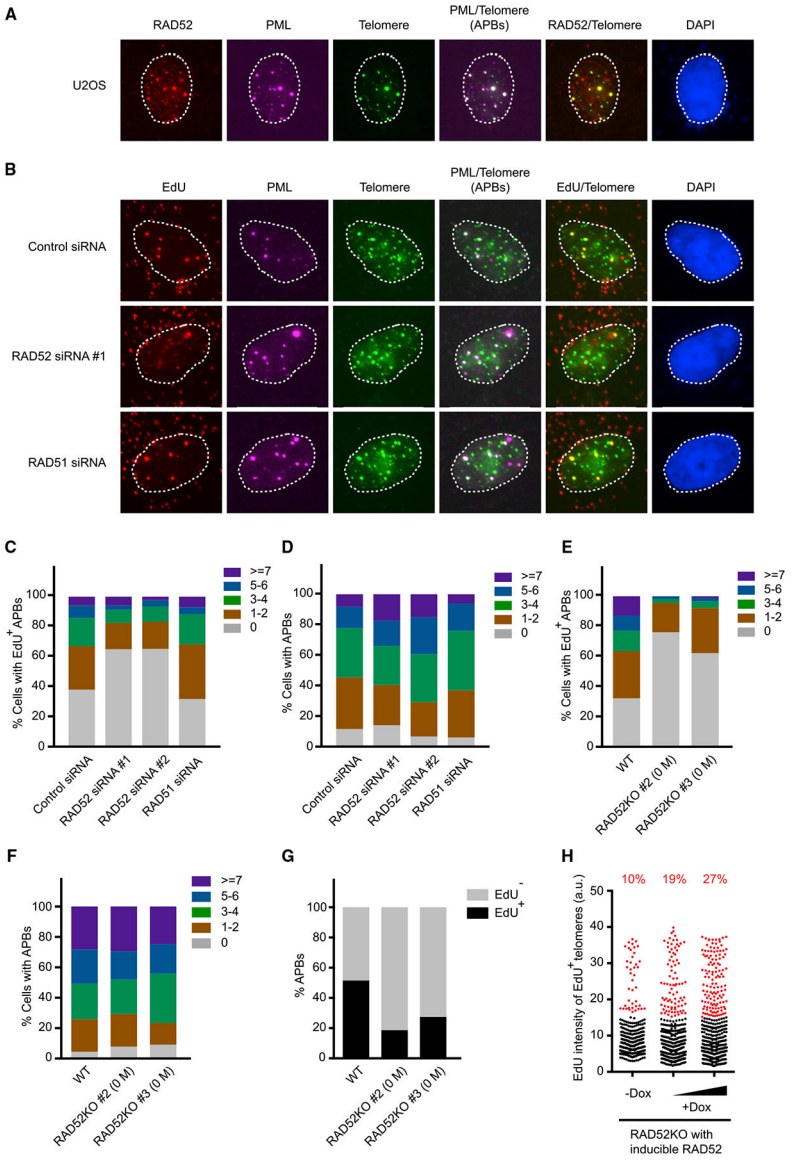

Figure 2. RAD52 but Not RAD51 Is Important for ALT Activity in APBs

(A) Representative images showing the localization of RAD52 to APBs in a G2 U2OS cell. Cells were synchronized in G2 using thymidine and CDK1i.

(B) Representative images showing incorporation of EdU in APBs in U2OS cells treated with control, RAD51, or RAD52 siRNA. Cells were synchronized in G2 using CDK1i.

(C and D) Approximately 100 cells analyzed in (B) were divided into five groups on the basis of the numbers of EdU^+ APBs (C) or total APBs (D).

(E and F) Wild-type (WT) and newly generated RAD52-KO U2OS cells were synchronized in G2 using thymidine and CDK1i, analyzed as in (B). Approximately 100 cells were divided into five groups on the basis of the numbers of EdU^+ APBs (E) or total APBs (F). RAD52-KO #2 and #3 are two independently generated cell lines. (0 M) indicates that the RAD52-KO cells were newly generated.

(G) Quantification of the EdU^+ APBs among total APBs in cells analyzed in (E) and (F).

(H) WT RAD52 was inducibly expressed in RAD52-KO cells with increasing concentrations of doxycycline (Dox). The total EdU signals of EdU^+ telomeres in >100 cells were quantified. The cells with total EdU signals of 15 a.u. or more were colored in red, and the fractions of these cells in the indicated cell populations were determined.

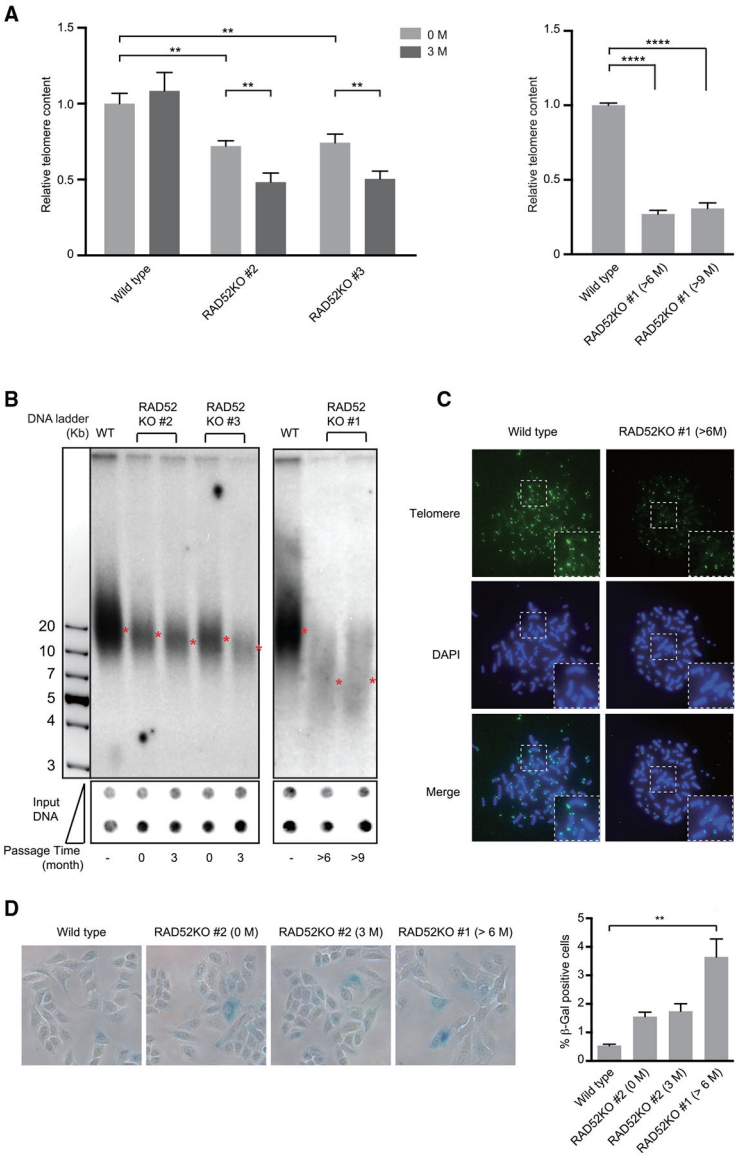

Figure 3. RAD52 Is Required for Telomere Maintenance in ALT$^+$ Cells

(A) Relative telomeric DNA contents determined by qPCR in WT U2OS cells, newly generated RAD52-KO cells, and RAD52-KO cells passaged for different lengths of time. 0 M, 3 M, > 6 M, and > 9 M indicates that the RAD52-KO cells have been passaged for 0, 3, >6, or >9 months, respectively. Error bars denote SD; n = 3 (experimental triplicates); *p < 0.05, **p < 0.01, ***p < 0.001, and ****p < 0.0001 (unpaired Student's t test).

(B) Telomere length was determined by TRF assay in WT U2OS cells, newly generated RAD52-KO cells, and RAD52-KO cells passaged for different lengths of time. Telomeres were detected by a 5' end-labeled $(CCCTAA)_3$ probe (top). Input genomic DNA was titrated and analyzed in anti-dsDNA dot blots and shown as loading controls (bottom).

(C) Telomere FISH of metaphase chromosomes of WT and extensively passaged RAD52-KO U2OS cells.

(D) WT U2OS cells and RAD52-KO cells passaged for different lengths of time were analyzed for senescence by β-galactosidase staining. Representative images of β-galactosidase staining (left) and quantifications of β-galactosidase-positive cells (right) are shown. Error bars denote SD; n = 3 (experimental triplicates); *p < 0.05, **p < 0.01, ***p < 0.001, and ****p < 0.0001 (unpaired Student's t test).

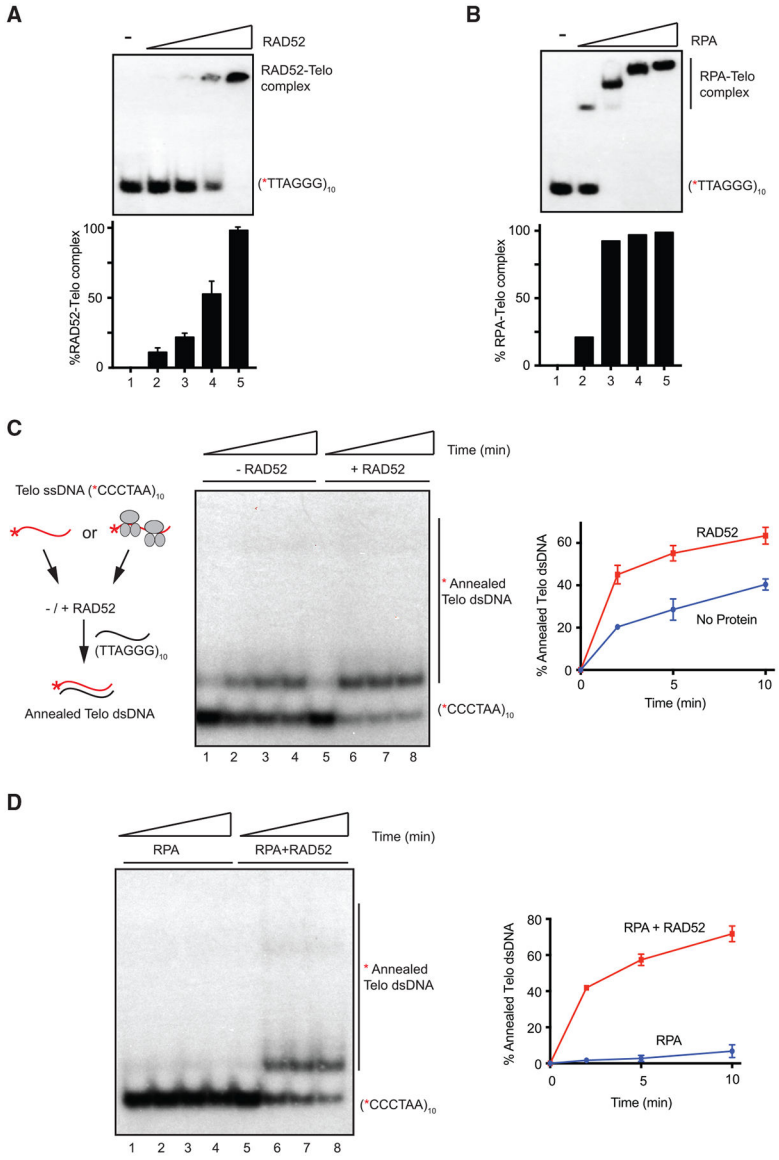

Figure 4. RAD52 Overcomes the Inhibition of Telomeric ssDNA Annealing by RPA

(A) End-labeled telomeric ssDNA (ssTelo, 20 nM) was incubated with RAD52 protein (80, 160, 320, and 640 nM) and analyzed for complex formation. The formation of DNA-protein complex was quantified according to the reduction in free ssTelo. Error bars denote SD; n = 3 (independent experiments).

(B) ssTelo (20 nM) was incubated with the RPA complex (20, 40, 80, and 160 nM) and analyzed as in (A).

(C and D) Telomeric ssDNA complementary to ssTelo $(CCCTTA)_{10}$ (40 nM) was end labeled, incubated without or with RPA (1 μM), and then incubated without or with RAD52 (1.4 μM). Unlabeled ssTelo $(TTAGGG)_{10}$ (40 nM) was added to the reactions. Reactions were carried out at 20°C in (C) or 27°C in (D), and stopped at 0, 2, 5, and 10 min. Annealing efficiency was determined by quantifying the remaining free probe after reactions.

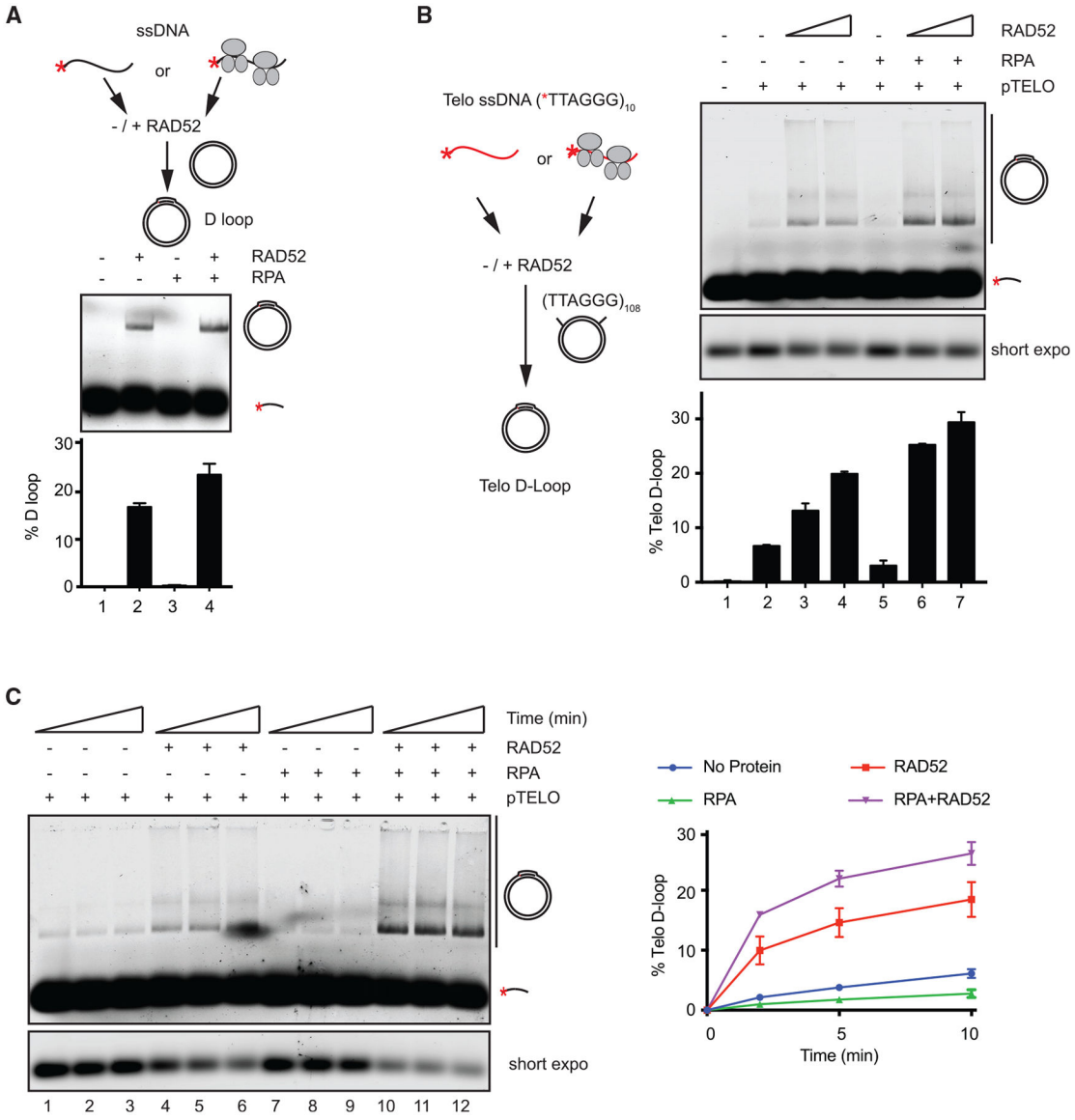

Figure 5. RAD52 but Not RAD51 Promotes Telomeric D-Loop Formation in the Presence of RPA

(A) An ssDNA oligomer with homologous sequences in the pBSDK+ plasmid (oligo 1, 30 nM) was end labeled. The probe was first coated with RPA (400 nM) or left uncoated, then sequentially incubated with RAD52 (1 μM) and the pBSK+ plasmid (25 nM). Error bars denote SD; n = 3 (independent experiments).

(B) End-labeled ssTelo (20 nM) was coated with RPA (200 nM) or left uncoated and then sequentially incubated with RAD52 (400 and 800 nM) and a plasmid containing 648 bp telomeric sequence (pTelo, 10 nM). The levels of telomeric D-loop formation were determined by quantifying the remaining free probe after reactions in the short exposure of the gel. Error bars denote SD; n = 3 (independent experiments).

(C) Telomeric D-loop formation was carried out as in (B) using the indicated proteins. The levels of telomeric D-loop formation were quantified at 0, 2, 5, and 10 min as in (B). Error bars denote SD; n = 3 (independent experiments).

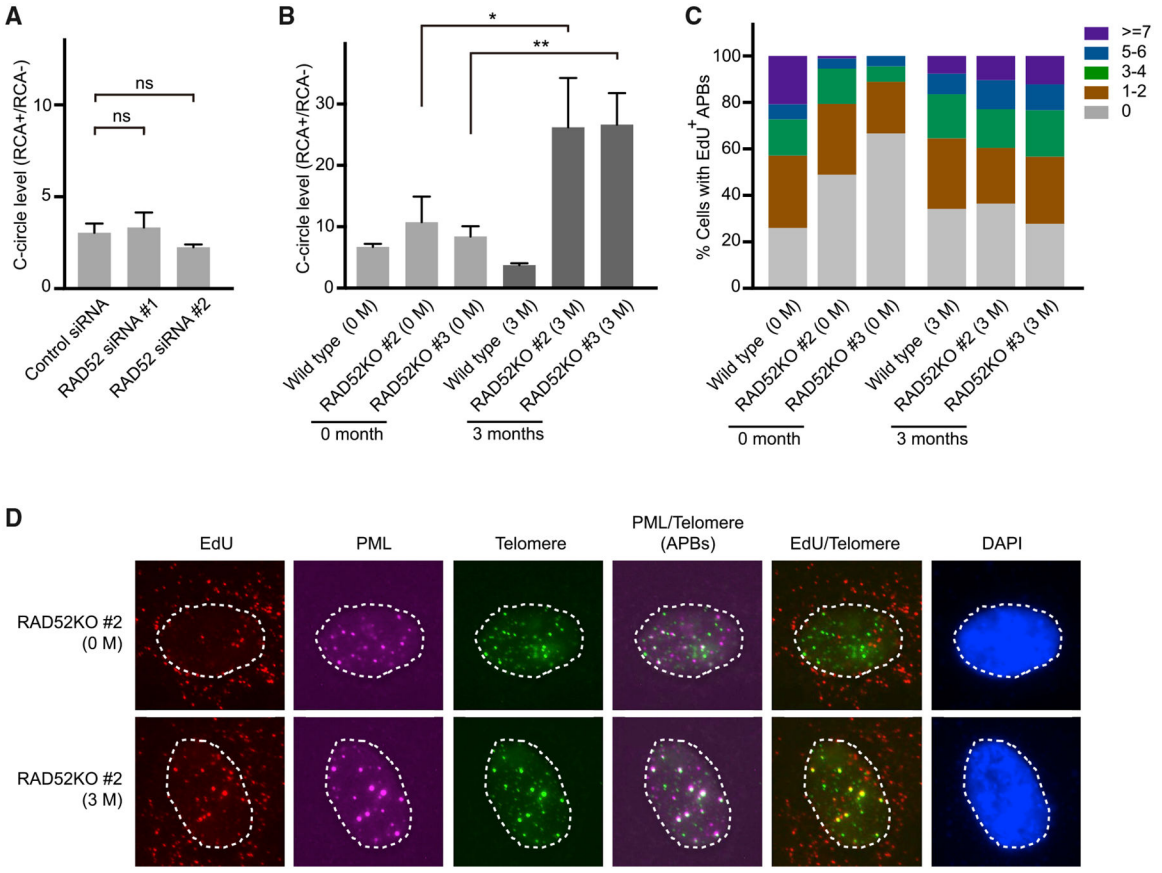

Figure 6. RAD52 Is Dispensable for C-Circle Formation

(A) Relative C-circle levels in U2OS cells transfected with control or RAD52 siRNA. Telomeric DNA contents were determined by qPCR with or without rolling-circle amplification (RCA) (see Figure S6B). The RCA+/RCA− ratios of samples reflect the relative levels of C-circle amplification. Error bars denote SD; n = 3 (experimental triplicates); ns, not significant (unpaired Student's t test).

(B) Relative C-circle levels in WT U2OS cells, newly generated RAD52-KO (0 M) cells, and passaged RAD52-KO (3 M) cells. Relative C-circle levels were determined as in (A). Error bars denote SD; n = 3 (experimental triplicates); *p < 0.05, **p < 0.01, ***p < 0.001, and ****p < 0.0001 (unpaired Student's t test).

(C) WT U2OS cells, newly generated RAD52-KO (0 M) cells, and passaged RAD52-KO (3 M) cells were synchronized in G2 using thymidine and CDK1i. Approximately 100 cells were divided into five groups on the basis of the numbers of EdU^+ APBs.

(D) Representative images of the RAD52-KO cells analyzed in (C).

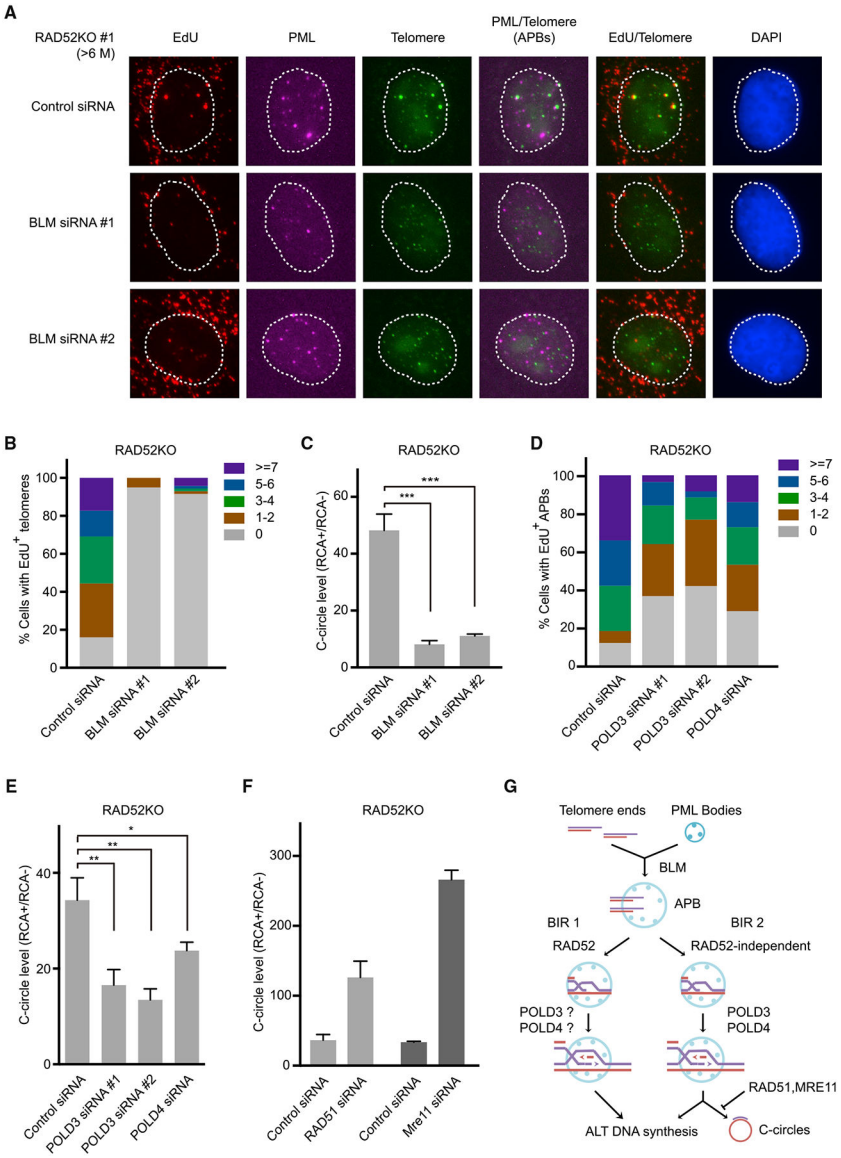

Figure 7. The RAD52-Independent ALT Pathway Is Mediated by BLM and POLD3/4

(A) Representative images showing EdU incorporation in APBs in extensively passaged RAD52-KO U2OS cells. Cells were treated with control or BLM siRNA and synchronized in G2 using CDK1i.

(B) Approximately 100 cells analyzed in (A) were divided into five groups on the basis of the numbers of EdU^+ telomeres.

(C) Relative C-circle levels in extensively passaged RAD52-KO cells transfected with control or BLM siRNA. Error bars denote SD; n = 3 (experimental triplicates); *p < 0.05, **p < 0.01, ***p < 0.001, and ****p < 0.0001 (unpaired Student's t test).

(D) Extensively passaged RAD52-KO cells were transfected with control, POLD3, or POLD4 siRNA and synchronized in G2 by CDK1i. Approximately 100 cells were divided into five groups on the basis of the numbers of EdU^+ APBs.

(E) Relative C-circle levels in extensively passaged RAD52-KO cells transfected with control, POLD3, or POLD4 siRNA. Quantification was done as in (C).
(F) Relative C-circle levels in extensively passaged RAD52-KO cells treated with control, RAD51, or MRE11 siRNA were analyzed as in (C).
(G) A model of the bifurcated framework of the ALT pathway.

KEY RESOURCES TABLE

REAGENT or RESOURCE	SOURCE	IDENTIFIER
Antibodies		
RAD52	Santa Cruz	Cat# sc-8350; RRID:AB_2284949
RAD51	Santa Cruz	Cat# sc-8349; RRID:AB_2253533
POLD3	Bethyl	Cat# A301–244A; RRID:AB_890596
POLD4	Novus Biologicals	Cat# H00057804-M01A; RRID:AB_2166594
BLM	Bethyl	Cat# A300–110A; RRID:AB_2064794
GAPDH	Millipore	Cat# ABS16; RRID:AB_10806772
PML	Abcam	Cat# ab96051; RRID:AB_10679887
Biotin	Abcam	Cat# ab53494; RRID:AB_867860
Chemicals, and Recombinant Proteins		
T4 polynucleotide Kinase	NEB	M0201S
Proteinase K	Thermo Fischer	25530049
Thymidine	Sigma	T1895–5G
CDKi (RO-3306)	Selleckchem	S7747
BSA	NEB	B9000S
ATP gamma P32	Perkin Elmer	NEG002250uc
IPTG	Calbiochem	420322
Ni^{2}+-NTA beads	QIAGEN	30230
Affi-Gel Blue Gel	BioRad	1537301
Click-iT EdU Alexa Fluor 488 Imaging Kit	Thermo Fischer	C10337
TelC-FITC	PNA Bio	F1009
Dextran Sulfate sodium	Sigma	D8906–10G
Formamide	Sigma	47671–1L-F
20× SSC	Thermo Fischer	AM9763
Azide-PEG3-Biotin	Sigma	762024–10MG
phi29 DNA Polymerase	NEB	M0269L
dNTP Set(100 mM)	Thermo Fischer	10297018
PureLink Genomic DNA Mini Kit	Thermo Fischer	K182002
Sequence-Based Reagents		

REAGENT or RESOURCE	SOURCE	IDENTIFIER
siRNA	This Study	See Table S1
Primers for C circle	This Study	See Table S2
Oligos for *in vitro* substrates preparation	This study	See Table S3
Software and Algorithms		
Image Lab	BioRad	http://www.bio-rad.com/en-us/product/image-lab-software
NIS element viewer	Nikon	https://www.nikoninstruments.com/Products/Software/NIS-Elements-Advanced-Research/NIS-Elements-Viewer